ACS OMEGA

Open Access

http://pubs.acs.org/journal/acsodf

Article

Toward Precise Modeling of Dopamine Release Kinetics: Comparison and Validation of Kinetic Models Using Voltammetry

Abhinav Goyal, Una Karanovic, Charles D. Blaha, Kendall H. Lee, Hojin Shin,* and Yoonbae Oh*

Cite This: *ACS Omega* 2024, 9, 33563−33573

Read Online

ACCESS | Metrics & More | Article Recommendations | Supporting Information

ABSTRACT: Dopamine (DA) is a neurotransmitter present within the animal brain that is responsible for a wide range of physiologic functions, including motivation, reward, and movement control. Changes or dysfunction in the dynamics of DA release are thought to play a pivotal role in regulating various physiological and behavioral processes, as well as leading to neuropsychiatric diseases. Therefore, it is of fundamental interest to neuroscientists to understand and accurately model the kinetics that govern dopaminergic neurotransmission. In the past several decades, many mathematical models have been proposed to attempt to capture the biologic parameters that govern dopaminergic kinetics, with each model seeking to improve upon a previous model. In this review, each of these models are derived, and the ability of each model to properly fit two fast-scan cyclic voltammetry (FSCV) data sets will be demonstrated and discussed. The dopamine oxidation current in both FSCV data sets exhibits hang-up and overshoot behaviors, which have traditionally been difficult for mathematical models to capture. We show that more recent models are better able to model DA release that exhibits these behaviors but that no single model is clearly the best. Rather, models should be selected based on their mathematical properties to best fit the FSCV data one is trying to model. Developing such differential equation models to describe the kinetics of DA release from the synapse confers significant applications both for advancing scientific understanding of DA neurotransmission and for advancing clinical ability to treat neuropsychiatric diseases.

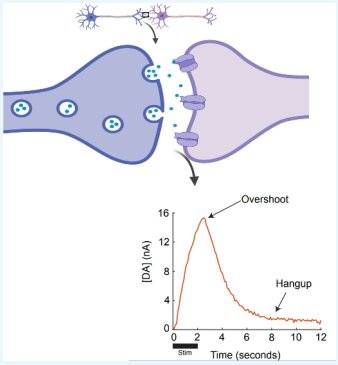

1. INTRODUCTION

Dopamine (DA) is a catecholamine neurotransmitter present within the mammalian brain that is responsible for a wide range of functions, including incentive motivation, addiction, memory and learning, and movement control.[1−3] Imbalances in DA extracellular concentration or transmission have been implicated in various neurologic and psychiatric diseases, including Parkinson's disease,[4−6] Alzheimer's disease,[7,8] Tourette's syndrome,[9] and Schizophrenia.[10] While DA does act on postsynaptic receptors within the same synapse it is released into, the majority of its effects are seen when it diffuses into the extracellular space to act on receptors on distant neurons.[11,12] This diffusion is a complex process governed by a variety of biological parameters, and it is of fundamental interest to neuroscientists to understand the kinetics that govern dopaminergic transmission.

Dopaminergic neurons are often thought to exhibit two modes of firing: low-frequency spontaneous pacemaker-like firing, and higher-frequency burst firing.[13−15] Physiologically, burst firing is thought to be used by dopaminergic neurons to encode salient environmental stimuli and leads to a robust phasic release of dopamine from synaptic terminals.[16] Fast-scan cyclic voltammetry (FSCV) is a popular method for visualizing the phasic release of DA into terminal regions, such as the dorsal striatum and nucleus accumbens, among others.[17−20] Given the inability to ensure localization of the working electrode to within a single synapse, FSCV is thought to measure the amount of DA that overflows from several surrounding synapses.

FSCV has been discussed in depth in many prior reviews;[17,21] briefly, FSCV takes advantage of the fact that different molecules are oxidized and reduced at specific voltages, which depends on their functional groups. As a catecholamine, DA is oxidized at around 0.6 V to its quinone form (dopamine-*o*-quinone), which is reduced at around −0.2 V at a scan rate of 400 V/s. Applying an electrical waveform that sweeps through these voltages will elicit release of current that is directly proportional to the concentration of DA present near the recording electrode. However, because FSCV relies on a rolling background subtraction method to exclude non-Faradaic current and other noise sources from the computation, it is restricted to measuring phasic, rather than tonic, levels of DA. To this end, researchers use FSCV to measure such phasic dopamine release, which is often elicited through electrical stimulation of axons afferent to these terminal regions, including those of the medial forebrain

Received: February 9, 2024
Revised: July 12, 2024
Accepted: July 18, 2024
Published: July 24, 2024

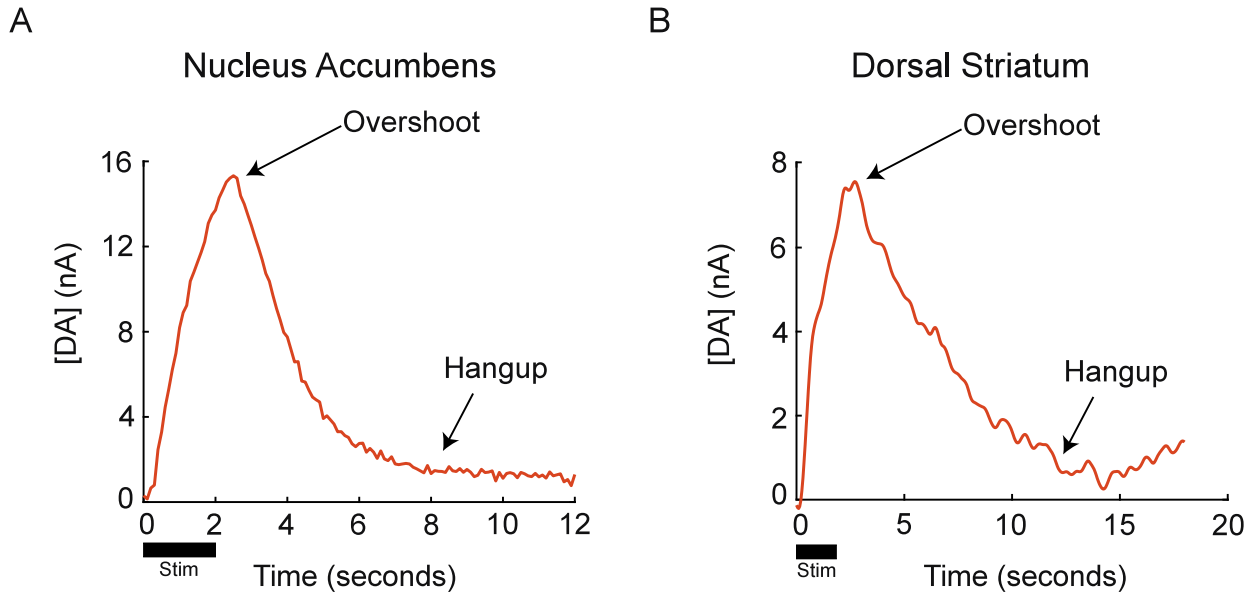

Figure 1. FSCV Data. (A) Evoked DA release in the nucleus accumbens with overshoot and hang-up labeled. (B) Same but for evoked DA release in the dorsal striatum.

bundle (MFB), substantia nigra, or ventral tegmental area (VTA).

Dopamine release kinetics measured using FSCV exhibit distinct characteristics in the nucleus accumbens compared to the dorsal striatum, reflecting the nuanced roles of these brain regions in reward and motor functions, respectively. DA release in the dorsal striatum has been shown to follow a patchwork of fast and slow domains which possess statistically different DA release and clearance profiles.[22−25] These different domains generate local variations in the tonic concentrations of DA. Increased tonic concentrations in certain regions provides autoinhibitory tone in the slow, but not fast, domains. In contrast, in the nucleus accumbens, while the presence of fast and slow release domains has been shown, an autoinhibitory tone by the presence of tonic concentrations of DA has not been found.[26] Further, DA clearance and overall kinetics have shown to be quite different compared to the dorsal striatum. Given the increasingly apparent relevance of these two brain regions to neuropsychiatric disorders involving reward, motivation, and motor planning, it was decided to focus on modeling release kinetics from these two regions specifically.

The ability to quantify phasic release of DA has several important applications, including modeling DA reuptake, synaptic overflow, and diffusion away from synapses (volume transmission), distinguishing between different types of dopaminergic release (e.g., fast vs slow), classifying the brain region based on dopaminergic release kinetics, and modeling the effects of pharmacologic agents on these kinetics. Several models have been proposed in recent decades to attempt to capture biologic parameters that govern dopaminergic kinetics. Many of these models are differential equations, with each successive model incorporating more terms to attempt to capture effects that a previous model was empirically determined to not adequately capture. In this study, each of these models will be discussed. The models will be divided into single-compartment models and multicompartment models, based on the assumptions that underlie their development.

2. MATERIALS AND METHODS

2.1. Electrode Fabrication. Carbon fiber microelectrodes (CFMs) were fabricated using an established standardized CFM design at Mayo Clinic.[20] A single carbon fiber (AS4, diameter = 7 μm; Hexel, Dublin, CA) was inserted into a silica tube (ID = 20 μm, OD = 90 μm, 10 μm coat with polyimide; Polymicro Technologies, Phoenix, AZ). The connection between the carbon fiber and the silica tubing was sealed with epoxy resin. The silica tubing was then attached to a nitinol (Nitinol #1, an alloy of nickel and titanium; Fort Wayne Metals, IN) extension wire with a silver-based conductive paste. The nitinol wire was then insulated with polyimide tubing (ID = 0.0089″, OD = 0.0134, WT = 0.00225; Vention Medical, Salem, NH) up to the exposed carbon fiber tip. The exposed carbon fiber was then trimmed under a dissecting microscope to a length of 50 μm. An Ag/AgCl reference electrode was prepared from Teflon-coated silver wire (A-M systems, Inc., Sequim, WA) by chlorinating the stripped tip in saline with a 9 V dry cell battery. CFMs were chemically tested in a beaker with TRIS buffer prior to coating with a PEDOT:Nafion deposition solution, which has been shown to minimize the effect of *in vivo* biofouling and increase sensitivity to electroactive monoamine neurotransmitters.[27]

2.2. In Vivo Data Acquisition. For each model, the derivation and underlying assumptions will be discussed, followed by an evaluation of the model on FSCV data acquired from six male Sprague−Dawley rats (Envigo; 150−200g). Rats were kept in social housing in an Association for Assessment and Accreditation of Laboratory Animal Care International (AAALAC) accredited vivarium following a standard 12-h light/dark cycle at constant temperature (21 °C) and humidity (45%) with ad libitum food and water. The present studies were approved by the Institutional Animal Care and Use Committee (IACUC), Mayo Clinic, Rochester, MN. The NIH Guide for the Care and Use of Laboratory Animals guidelines (Department of Health and Human Services, NIH publication No. 86−23, revised 1985) were followed for all aspects of animal care.

https://doi.org/10.1021/acsomega.4c01322
ACS Omega 2024, 9, 33563−33573

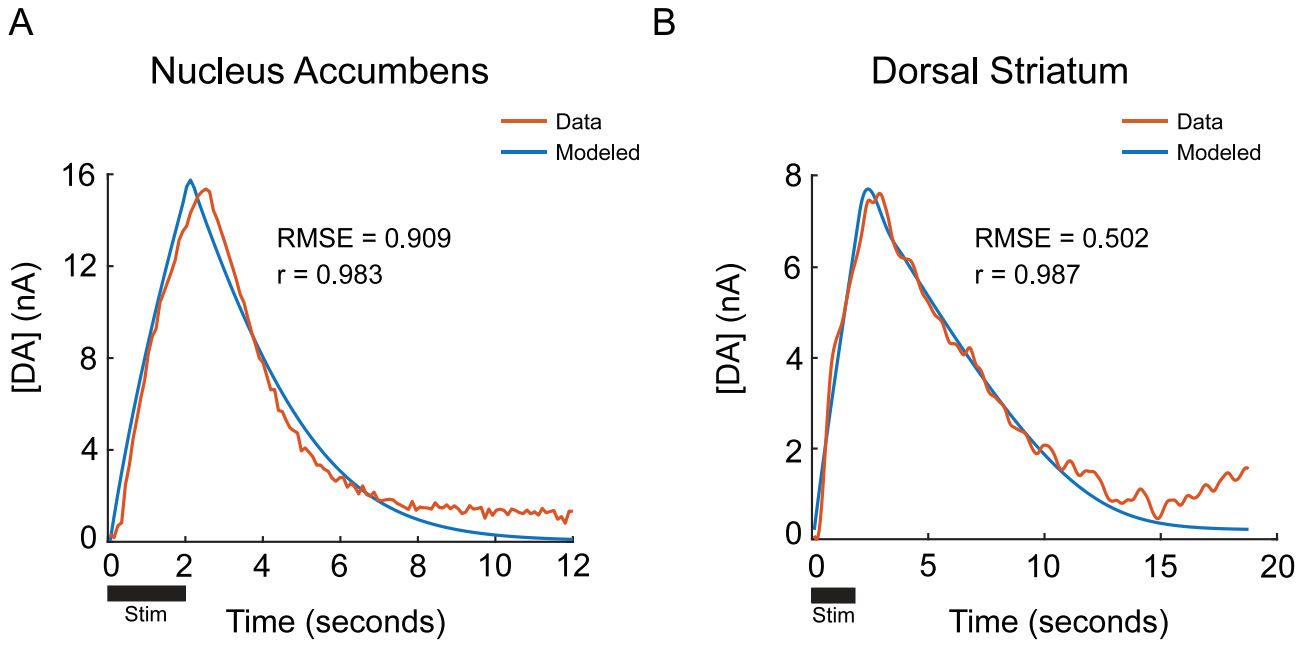

Figure 2. Wightman's original model. (A) Evoked DA release in the nucleus accumbens and associated modeled release by Wightman's original model. (B) Same but for evoked DA release in the dorsal striatum.

Rats were anesthetized with urethane (1.5 g/kg, i.p., Sigma-Aldrich, St. Louis, MO, USA). After depth of anesthesia was confirmed with loss of hind limb nociceptive withdrawal response, rats were fixed to a stereotactic surgical frame (David Kopf Instruments, Tujunga, CA, USA). A burr hole was drilled over either the right nucleus accumbens core (Coordinates from bregma:[28] AP: + 1.2, ML: + 1.4, DV: −6.5−7.5) or the right dorsal striatum (AP: + 2.0, ML: + 1.2, DV: −3.5−6) for placement of the CFM. Another burr hole was drilled on the contralateral side for placement of the Ag/AgCl reference electrode.

After the CFM was lowered to 2 mm above the target location, FSCV was activated. FSCV was run using the WINCS Harmoni using the WincsWare software.[29] FSCV was performed using a pyramidal voltage waveform (−0.4 V to +1.3 V) swept at 400 V/s at a 10 Hz scan rate. DA release was evoked by either 90 or 60 Hz stimulation (biphasic 2 ms pulse width, 0.3 mA, 2 s total stimulation) of the MFB (AP: −4.6, ML: + 0.9, DV: −6−8; Plastics One bipolar electrode, twisted) for dorsal striatum release, and of the VTA for nucleus accumbens release (AP: −5.3, ML: + 1.3, DV: −8; Plastics One bipolar electrode, concentric). Four of the data sets used 90 Hz stimulation, while the remaining two used 60 Hz stimulation. Stimulation was applied, and the resulting DA current was recorded. The CFM was then lowered by 0.1 mm. The process was repeated until maximal DA current was achieved by stimulation.

2.3. Data Processing. Data for this study were taken after the depth of optimal DA release was located.[18,19] The same data were used for all models to ensure fairness. From each FSCV data set, a representative evoked release was chosen that exhibited behaviors such as overshoot and hang-up to showcase the difference in each model's ability to account for such characteristics in the DA release profile (Figure 1). It should be noted that these data represent individual responses from brain regions that produce a wide variety of responses *in vivo*. Overshoot refers to continued rise in the FSCV oxidative current after electrical stimulation ends, while hang-up refers to a prolonged delay before the oxidative current returns to baseline after electrical stimulation ends.[30,31] Each signal was chosen such that the fit would begin immediately when stimulation began. The models were also fit on 4 additional data sets, 2 from the dorsal striatum and 2 from the nucleus accumbens. (see supplement).

The ability of each model to properly fit the FSCV data will be demonstrated and discussed. For this review, each model was generated in Matlab, and the parameters were optimized to fit each FSCV curve via an exhaustive grid search. Best-fit parameters are determined by the set of parameters that give the lowest root-mean square error (RMSE) between the model fit and the true data. Best-fit RMSEs and Pearson correlation coefficients are reported for each model fit. The Matlab code for each model has been made available on a public GitHub repository.

3. RESULTS

3.1. Single-Compartment Models. *3.1.1. Wightman's Original Model.* The first widely accepted mathematical model to govern DA kinetics was introduced in a paper by Wightman et al. in 1988.[32] They realized that the response to DA release seen via FSCV would depend on a variety of factors, including the material properties of the working electrode, the distance from the working electrode from the release sites, and the electrical stimulation parameters used to evoke DA release. After conducting a systematic series of experiments evaluating the effects of working electrode position, stimulus frequency, and stimulus duration, the authors proposed that the amount of DA detected by the working electrode from each stimulus pulse reflects a balance between DA release and DA reuptake (eq 1).

$$[\mathrm{DA}]_{\mathrm{detected}} = [\mathrm{DA}]_{\mathrm{p}} - [\mathrm{DA}]_{\mathrm{uptake}} \quad (1)$$

where $[\mathrm{DA}]_{\mathrm{p}}$ is the amount of DA released by the pulse and $[\mathrm{DA}]_{\mathrm{uptake}}$ is the amount of DA that is removed from the extracellular space by reuptake before reaching the working

https://doi.org/10.1021/acsomega.4c01322
ACS Omega 2024, 9, 33563−33573

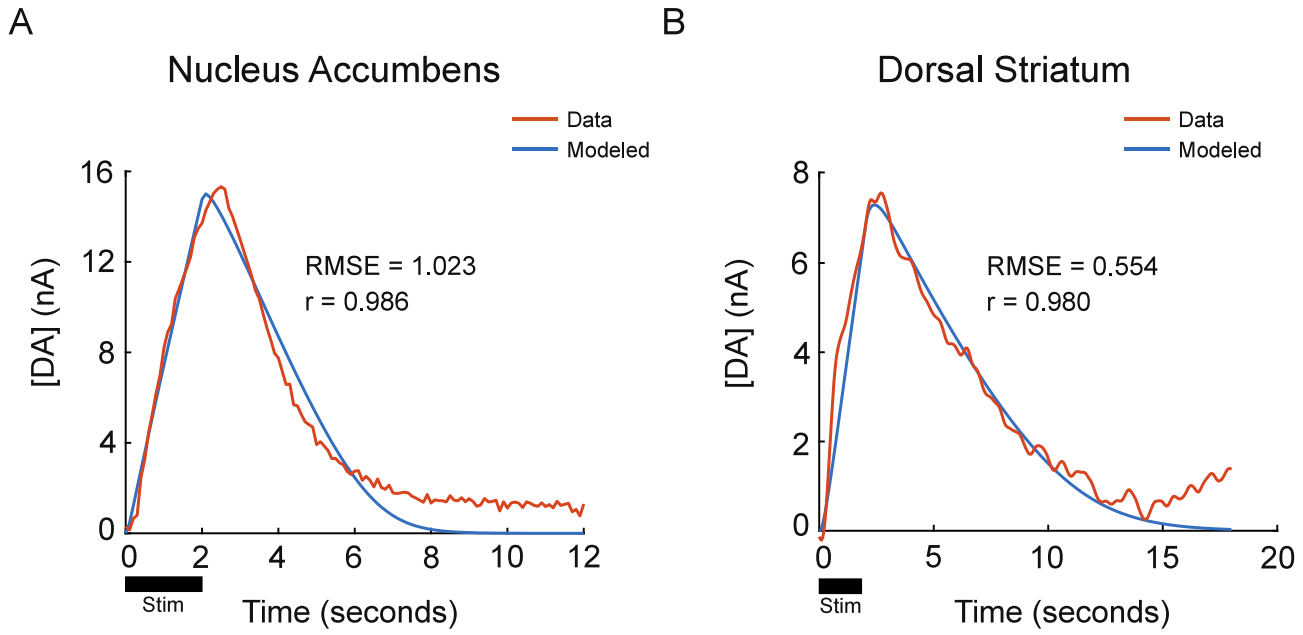

Figure 3. Diffusion gap model. (A) Evoked DA release in the nucleus accumbens and associated modeled release by the diffusion gap model. (B) Same but for evoked DA release in the dorsal striatum.

electrode. The authors then derive expressions for both terms on the right side by assuming a homogeneous single compartment surrounding the synapse and working electrode and that reuptake follows Michaelis–Menten kinetics.

$$[\mathrm{DA}]_{\mathrm{uptake}} = \int_0^t \frac{V_{\max}[\mathrm{DA}]}{K_m + [\mathrm{DA}]}$$

By assuming that the DA released per pulse is constant and independent of frequency, it is assumed that the sum of the DA released per pulse is the DA released at the first pulse multiplied by the number of pulses n over a time t. If the frequency of the pulse train is f, then $n = f \times t$.

$$\sum_{j=1}^{n} [\mathrm{DA}]_{\mathrm{p}} = ft[\mathrm{DA}]_{\mathrm{p},0}$$

By plugging these expressions for reuptake and release back into eq 1, the time dependence of DA sensed by the working electrode can be derived (eq 2):

$$[\mathrm{DA}](t) = ft[\mathrm{DA}]_{\mathrm{p},0} - \int_0^t \frac{V_{\max}[\mathrm{DA}]}{K_m + [\mathrm{DA}]}\mathrm{d}t \tag{2}$$

Differentiating this expression with respect to t yields the final rate expression that governs DA release (eq 3):

$$\frac{\mathrm{d}[\mathrm{DA}]}{\mathrm{d}t} = [\mathrm{DA}]_{\mathrm{p},0}f - \frac{V_{\max}[\mathrm{DA}]}{K_m + [\mathrm{DA}]} \tag{3}$$

It should be noted here that the first term drops to 0 after stimulation is terminated.

Figure 1 shows the best fit of Wightman's original model to the DA release evoked by stimulation in both the nucleus accumbens (Figure 2A) and dorsal striatum (Figure 2B). The respective best-fit kinetic parameters, as well as RMSE and Pearson correlation coefficients are also included with each plot.

As expected from such a simple differential model, the model fit does not properly account for the overshoot exhibited by the nucleus accumbens data, or the hang-up exhibited by both sets of data. Future models will seek to account for overshoot and hang-up, either by altering the model itself, or by altering the data.

3.1.2. Diffusion Gap Model. The diffusion gap model was also initially proposed by Wightman et al. in 1988 and remained the dominant model for decades. The diffusion gap model considers the tortuosity of DA diffusion through the extracellular space due to a physical gap between the site of DA release and the working electrode. To account for this gap, the diffusion gap model extends the previous single compartment model by adding in a diffusion operator derived from Fick's second law (eq 4):

$$\frac{\partial[\mathrm{DA}]}{\partial t} = D\frac{\partial^2[\mathrm{DA}]}{\partial x^2} + [\mathrm{DA}]_{\mathrm{p},0}f - \frac{V_{\max}[\mathrm{DA}]}{K_m + [\mathrm{DA}]} \tag{4}$$

where D is the diffusion constant of DA, and all other terms are as they were in eq 3. Equation 4, now a partial differential equation, is most easily solved by numerically estimating the solutions to the partial derivative term rather than seeking an analytical solution. This can be accomplished using a finite element method, which treats the spatial partial derivative as a series of finite differences along a predefined mesh. This transforms the partial derivative term into a system of ordinary differential equations (ODEs). The number of ODEs is determined by the number of columns of the mesh. In our implementation, finite element analysis was used to convert the parabolic term into a system of 20 ODEs, each representing a fixed distance from the working electrode. The system was solved with Matlab's ODE15s solver.

Alternatively, the diffusion operator can be solved analytically. Spillover of dopamine from a single vesicle can be modeled using this analytical solution, modified to include dopamine transporter (DAT)-mediated uptake and the structure of extracellular space:

https://doi.org/10.1021/acsomega.4c01322
ACS Omega 2024, 9, 33563−33573

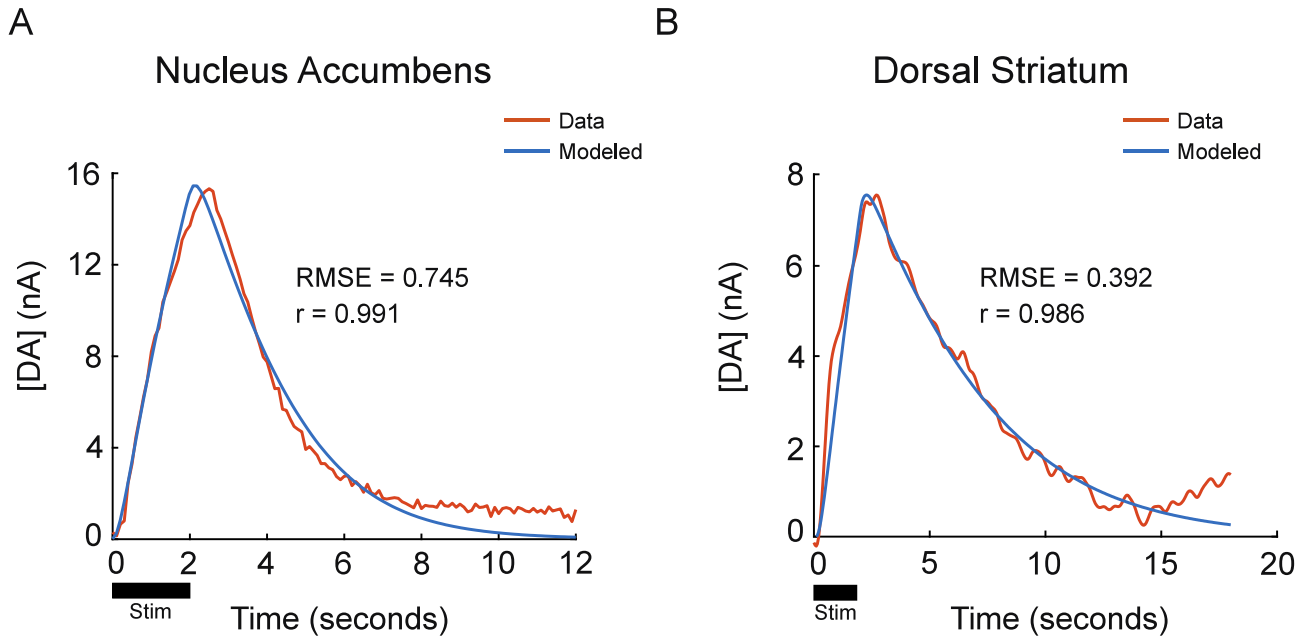

Figure 4. Restricted diffusion model. (A) Evoked DA release in the nucleus accumbens and associated modeled release by the restricted diffusion model. (B) Same but for evoked DA release in the dorsal striatum.

$$C(r, t) = \frac{UC_f}{\alpha(4D^* t\pi)^{3/2}} e^{-r^2/4D^* t - k' t}$$

Where $C(r,t)$ gives the extracellular DA concentration as a function of position (r) and time (t) after release, U is the volume of the vesicle, C_f is the fill concentration per vesicle, and α is the extracellular volume fraction. The diffusion constant D is reduced by tortuosity λ to an apparent diffusion constant $D^* = D/\lambda$. DAT-mediated uptake is taken into account by including the k' reuptake constant, where $k' = V_{max}/K_m$. For this paper, we used finite element analysis to numerically build up solutions to eq 4.

The diffusion gap model is slightly better at accounting for the overshoot exhibited by the nucleus accumbens data than Wightman's original model was, likely owing to the diffusion operator's ability to consider the continued increase of DA after stimulation ends by accounting for spatial diffusion (Figure 3). However, it performs worse than Wightman's original model later in the data set during the hang-up phase, as the diffusion gap model asymptotically trends toward 0 toward the end of the number of provided iteration cycles. In both cases, the overall RMSE was higher for the diffusion gap model than Wightman's original model, likely due to diffusion gap's very poor fit during the hang-up phase.

3.2. Multiple Compartment Models. *3.2.1. Restricted Diffusion Model.* The restricted diffusion model was set forth by Walters et al. in 2014,[30] in an attempt to better account for the overshoot and hang-up present in real FSCV data than prior single-compartment models. Additionally, single-compartment models are unable to account for multiple DA signals (e.g., fast and slow DA domains) present at once. To account for these various factors, Walters et al. proposed that the synapse-electrode system consists of 2 compartments. The fundamental difference between single- and multicompartment models is that the latter assumes that DA does not diffuse freely through extracellular space to reach the working electrode. Rather, DA is released into the "inner compartment," and is only detected by the working electrode when it diffuses into the "outer compartment." The time that DA spends within the inner compartment theoretically should account for the overshoot and hang-up seen in FSCV data. These ideas built off of work by Nicholson and colleagues who established several potential mechanisms of restricted diffusion, including the presence of dead space microdomains[33] that trap diffusing molecules, the obstruction of passageways by macromolecules, and the presence of specific[34] or nonspecific[35] binding sites to bind and impede the diffusing molecule.

Since the restricted diffusion model is a multicompartment model, it consists of a system of two ODEs:

$$\frac{dDA_{ic}}{dt} = DA_{p,0} f - DA_{ic} T \quad (5)$$

$$\frac{d[DA]_{oc}}{dt} = \frac{DA_{ic} T}{V_{oc}} - \frac{V_{max}[DA]_{oc}}{[DA]_{oc} + K_m} \quad (6)$$

Here, DA_{ic} is the number of moles trapped in the inner compartment, $[DA]_{oc}$ is the concentration of DA trapped in the outer compartment, V_{oc} is the volume of the outer compartment, T is a first-order reaction rate constant describing the transport between the inner and outer compartments, and all other terms are defined as in eq 3. This model may be tuned to each FSCV data set by optimizing $DA_{p,0}$, T, K_m, and V_{max}.

Figure 4 shows the performance of the restricted diffusion model on nucleus accumbens and dorsal striatum data.

The restricted diffusion model as presented captures the overall behavior of the DA release from both data sets better than either single-compartment model, as evidenced by the lower RMSEs and higher Pearson coefficients. However, it continues to fail to properly capture the overshoot seen in the nucleus accumbens data or the hang-up in either data set (Figure 4).

3.2.2. Modified Restricted Diffusion Model. In the following year, Walters et al. published a modified version of

https://doi.org/10.1021/acsomega.4c01322
ACS Omega 2024, 9, 33563−33573

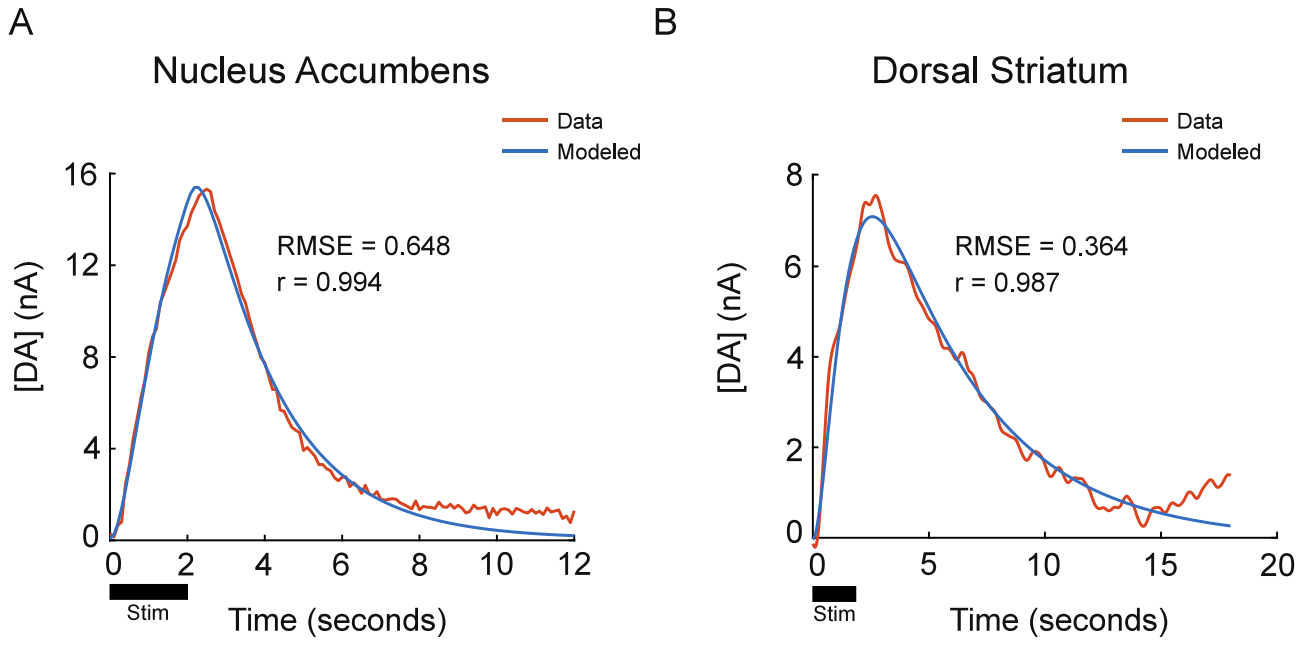

Figure 5. Modified restricted diffusion model. (A) Evoked DA release in the nucleus accumbens and associated modeled release by the modified restricted diffusion model. (B) Same but for evoked DA release in the dorsal striatum.

the restricted diffusion model to better account for the hang-up and overshoot in FSCV data.[31] First, Walters et al. modified eqs 5 and 6 to assume that transport between the inner and outer compartments obeys first order kinetics:

$$\frac{\mathrm{dDA_{ic}}}{\mathrm{d}t} = \mathrm{DA_{p,0}} f e^{-k_r t} - \mathrm{DA_{ic}} T \tag{7}$$

$$\frac{\mathrm{d[DA]_{oc}}}{\mathrm{d}t} = \frac{\mathrm{DA_{ic}} T}{V_{oc}} - [\mathrm{DA}]_{oc} k_u \tag{8}$$

In this set of equations, k_r is the first-order rate constant that modifies DA release, and k_u is the first-order rate constant for DA reuptake. All other terms are defined as in eqs 5 and 6. In eqs 7 and 8, the model may be tuned to fit FSCV data by optimizing k_r, k_u, T, and $\mathrm{DA_{p,0}}$.

The modification of the restricted diffusion model does allow the model to better capture the overshoot behavior exhibited by the nucleus accumbens data (Figure 5A). It seems to perform better overall at modeling the nucleus accumbens data. Similarly, the model underestimates the peak of the dorsal striatum data, but better fits the hang-up behavior at the end (Figure 5B). Overall, from these two data sets, it is unclear that the modified restricted diffusion model significantly outperforms the original, but it does yield slightly lower RMSEs and higher Pearson coefficients.

3.2.3. Modified Restricted Diffusion Model with Hang-up Correction. Next, in the same work, Walters et al. discuss that the hang-up behavior is due to DA adsorption to the working electrode and developed a method to subtract out this hang-up component from the FSCV signal. They modeled the hang-up component as

$$\frac{\mathrm{d}H}{\mathrm{d}t} = k_{ads}[\mathrm{DA}] - k_{des}\Gamma_{\mathrm{DA}} \tag{9}$$

Here, H is the hang-up component, the k terms represent the rate constants for adsorption and desorption, respectively, [DA] represents the concentration of DA at the working electrode, and Γ_{DA} is a measure of the coverage of DA on the electrode surface.[36] The original authors used a finite difference model to approximate the hang-up component; in our implementation we used Matlab's ODE45 solver to fit the model to our FSCV data. The model is fit to the whole data; however, only the time window that contains the putative hang-up is used to tune the parameters (Figure 6).

The hang-up correction is instrumental in improving model fit to both sets of data, yielding the lowest RMSEs and highest Pearson coefficients thus far. By combining the ability of the modified restricted diffusion model to account for overshoot behavior with the hang-up correction fit, a high correlation fit can be made, especially to the nucleus accumbens data. For the dorsal striatum data, the model consistently underestimates the middle phase of the data, prior to the hang-up component.

3.2.4. Three Compartment Model. The most recently proposed model governing DA release in response to electrical stimulation was proposed by Trevathan and colleagues in 2017.[37] This model extends the restricted diffusion model to incorporate a third compartment, and it divides the tunable parameters into subject-specific parameters that only need to be trained once per animal (transport and reuptake parameters) and response-specific parameters that are trained for each evoked response (DA release per pulse). Notably, the restricted diffusion model does not perform well when the transport and reuptake parameters are trained in a subject-specific manner, which motivated Trevathan and colleagues to develop the three-compartment model.

According to this model, during stimulation, DA is simultaneously released at a constant rate into compartment 1 and at an exponentially decaying rate into compartment 2. The authors propose that compartments 1 and 2 could model the slow and fast DA domains, respectively, seen in the dorsal striatum and nucleus accumbens.[30,31,37] Dopamine then diffuses from compartments 1 and 2 into compartment 3, where the working electrode is located, following the principles of restricted diffusion. The model consists of a system of three coupled ODEs:

https://doi.org/10.1021/acsomega.4c01322
ACS Omega 2024, 9, 33563−33573

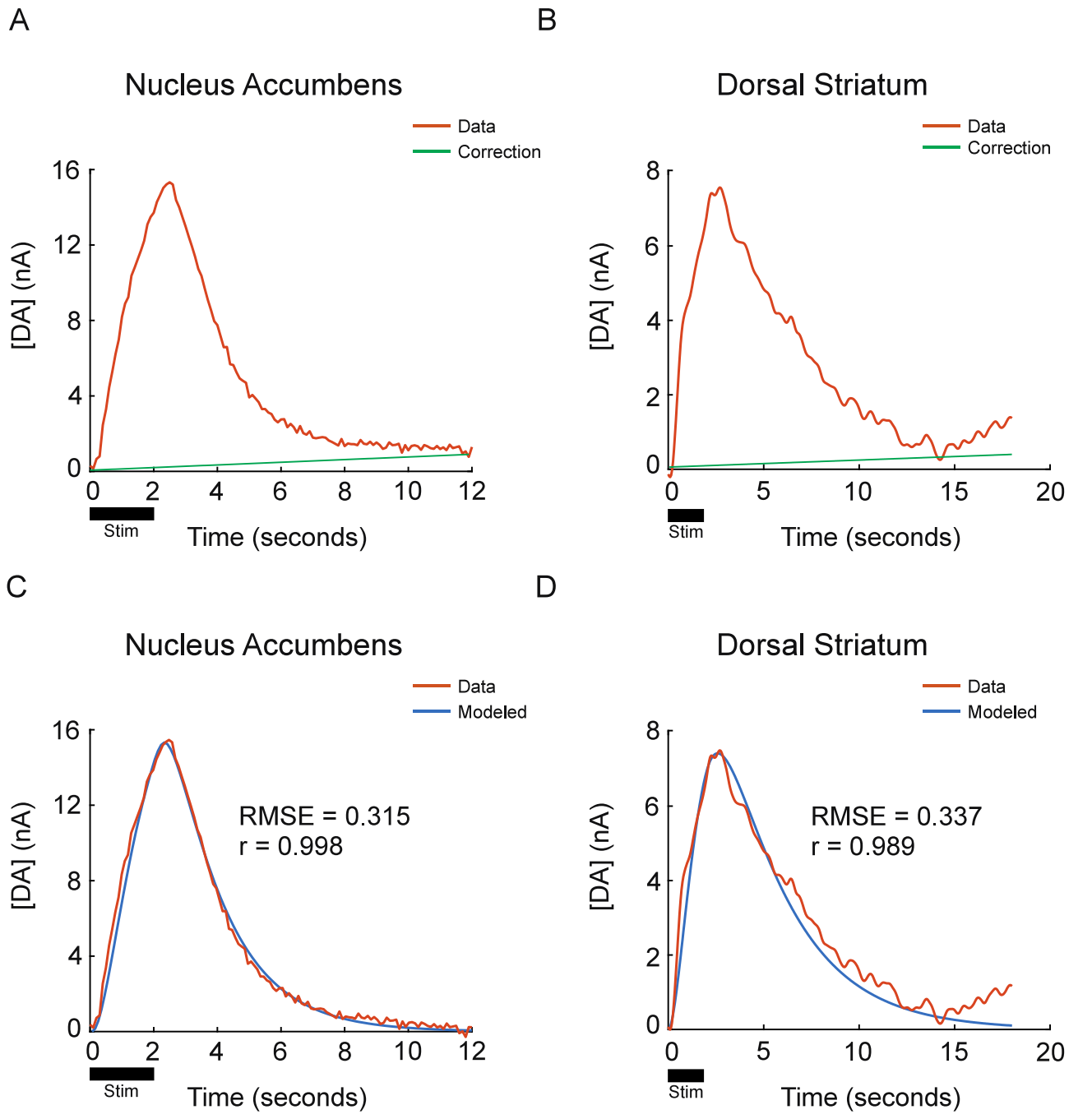

Figure 6. Modified restricted diffusion model with hang-up correction. (A) Evoked DA release in the nucleus accumbens and associated hang-up correction. (B) Same but for evoked DA release in the dorsal striatum. (C) Evoked DA release in the nucleus accumbens and associated modeled release by the modified restricted diffusion model after the hang-up component was subtracted out. (D) Same but for evoked DA release in the dorsal striatum.

$$\frac{d[DA]_{C1}}{dt} = [DA]_{p1,0} f - [DA]_{C1} T_1 \quad (10)$$

$$\frac{d[DA]_{C2}}{dt} = [DA]_{p2,0} f e^{-Qt} - [DA]_{C2} T_2 \quad (11)$$

$$\frac{d[DA]_{C3}}{dt} = \frac{[DA]_{C1} T_1 + [DA]_{C2} T_2}{V_{C3}} - \frac{V_{max}[DA]_{C3}}{[DA]_{C3} + K_m} \quad (12)$$

Here, Q is a tunable parameter that models the rate of attenuation of the release of DA into C2, T_1 and T_2 are the first-order rate constants modeling transport of dopamine from C1 and C2, respectively, into C3, and all other terms are as they have been defined previously.

The primary advantage of this model is that, after training the subject-specific parameters once, each subsequently evoked response requires training of only two response-specific parameters (the two $[DA]_p$ terms), dramatically lowering computation time. This reduced computation time is of vital importance when designing algorithms for real-time monitoring or closed-loop modulation of DA release.

https://doi.org/10.1021/acsomega.4c01322
ACS Omega 2024, 9, 33563−33573

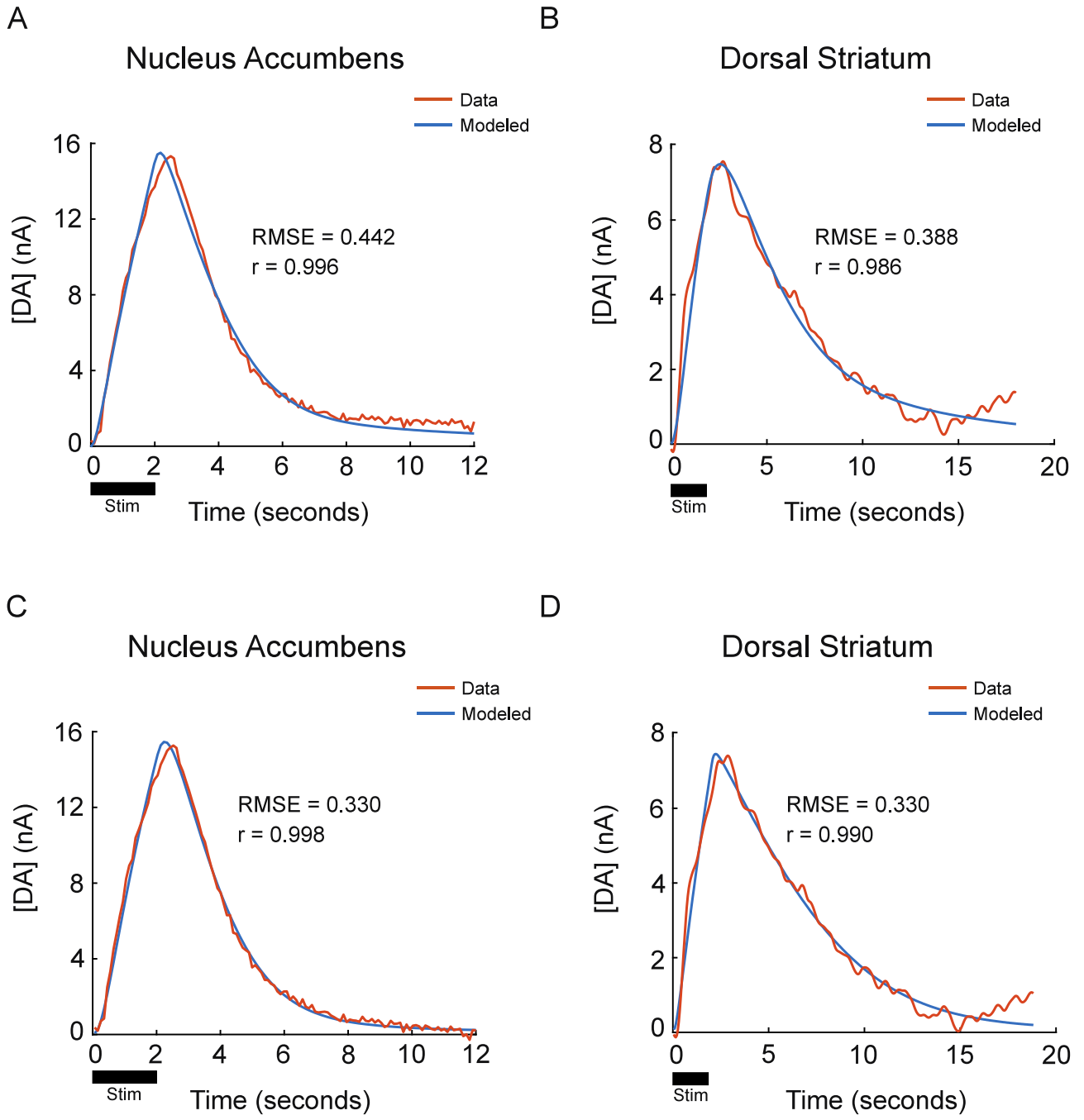

Figure 7. Three compartment model. (A) Evoked DA release in the nucleus accumbens and associated modeled release by the three compartment model. (B) Same but for evoked DA release in the dorsal striatum. (C) Evoked DA release in the nucleus accumbens and associated modeled release by the three compartment model after the hang-up component was subtracted out. (D) Same but for evoked DA release in the dorsal striatum.

The three compartment model once again fails to account for the overshoot behavior exhibited by the nucleus accumbens data, but much better accounts for the hang-up in both data sets. Overall it performs similarly (striatum) or better than (nucleus accumbens) the modified restricted diffusion model alone, but the hang-up correction in combination with the modified restricted diffusion model has given the best fits thus far (Figure 7A,B).

3.2.5. Three Compartment Model with Hang-up Correction. It is seen that the hang-up correction may potentially be a useful tool to smooth out the end of the DA release profile whenever hang-up is seen. This correction term is not necessarily an innate component of the restricted diffusion model. We believe that, by performing an initial hang-up correction to data sets that possess a hang-up component, the fit of the resulting model will be improved. We have attempted this by first performing a hang-up correction on our data sets and then attempting to fit the data with the three compartment model. Here, the same hang-up correction was used as previously (Figure 6).

This combined model outperforms the modified restricted diffusion combined model for fitting the dorsal striatum data, as it better captures the middle phase of the data before the hang-up component, and it performs similarly for fitting the

https://doi.org/10.1021/acsomega.4c01322
ACS Omega 2024, 9, 33563−33573

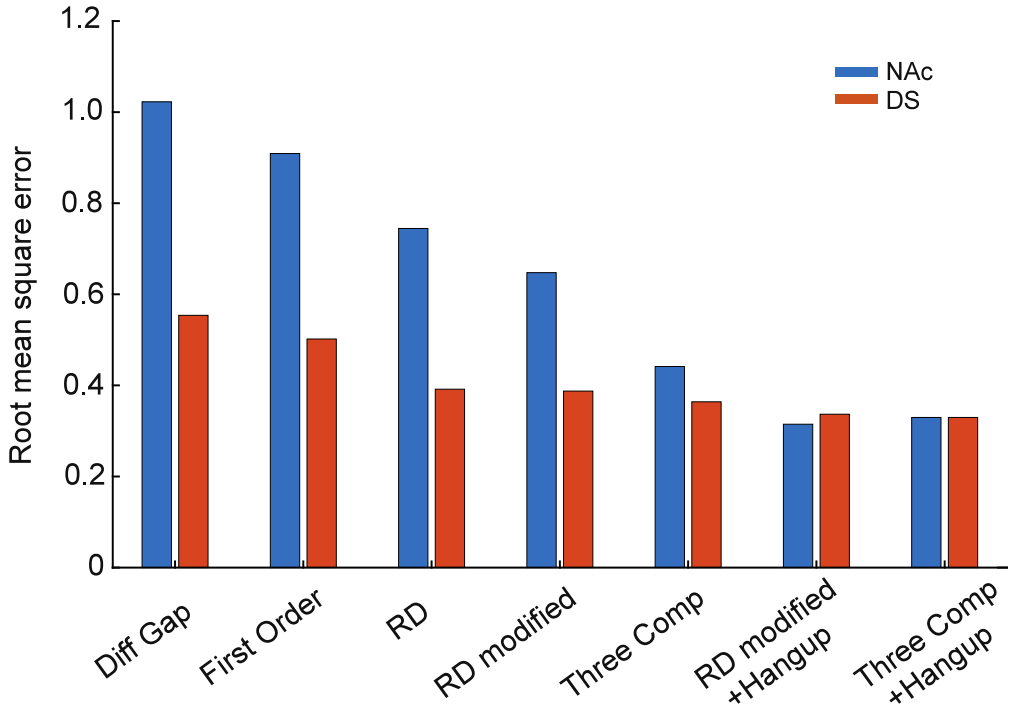

Figure 8. Root mean square errors across methods. RMSEs between the true and modeled dopamine release curves for both data sets across models.

nucleus accumbens data, though it is slightly worse at fitting the overshoot phase (Figure 7C,D).

Figure 8 shows the overall root-mean-square errors of each of the models for the nucleus accumbens and dorsal striatal data. In general, the trends are as expected; as additional features and complexity are added to each model, the error between the model fit and the true data tended to decrease. Exceptions to this include diffusion gap having a higher RMSE than the first order model, and this is attributed to the diffusion gap fit being forced to asymptotically trend toward 0 after stimulation ends, leading to a poor fit to hang-up behavior. Further, the modified restricted diffusion model with hang-up correction performed better than the more complex three compartment model.

4. DISCUSSION

This work sought to summarize the models set forth in the past for modeling DA release kinetics during FSCV experiments. For each model, the mathematical derivation was provided, along with rationale for its creation and how it might better be able to capture a component of the DA release profile that previous models failed to capture. Each model was then used to generate release kinetics for 6 FSCV data sets from our lab, including 3 from the nucleus accumbens and 3 from the dorsal striatum, across 2 different electrical stimulation frequencies. By directly comparing all of these models on the same data sets, the specific benefits and drawbacks of each model can be quantitatively showcased.

Overall, it seems that no single model can be considered to be the best for fitting all FSCV DA release data. Rather, certain models seem to be better suited toward modeling data sets that contain specific features. For example, by incorporating assumptions derived from knowledge about the physiology of DA diffusion, including the likely presence of multiple compartments and the presence of molecules, binding sites, etc. that would impede the diffusion of DA, the restricted diffusion models are better able to capture the overall release profile than the single-compartment models; however, the hang-up component of release profiles was still not properly accounted for until the hang-up correction was introduced. After understanding that the hang-up was a feature of DA adsorption to the CFM electrode, and not a feature of DA diffusion physiology, a correction term was derived; by subtracting out this adsorption component, the data could then be better fit.

It is also seen that features of each model can be combined to match the features present within a specific data set. For example, hang-up correction can be applied to any model, while the three-compartment model boasts the benefit of only needing 3 of its 7 parameters trained for additional data sets from the same animal. By incorporating the hang-up correction to the three-compartment model, the benefits of both can be retained—the speed of fitting with the three compartment model can be combined with the fit accuracy obtained after subtracting out the hang-up component where present.

The dorsal striatum and the nucleus accumbens, the two brain regions investigated within this and many similar works in the past, are critical regions within the limbic system of the brain.[38−41] They possess many important physiological functions as part of the limbic system; however, their dysfunction has also been shown to underlie the pathophysiology of many neurological and neuropsychiatric disorders. The dorsal striatum, integral to motor control and habit formation, is implicated in disorders such as Parkinson's disease, Huntington's disease, and obsessive-compulsive disorder, where disruptions in motor function and repetitive behaviors are prominent.[4,14] The nucleus accumbens, which primarily controls reward processing and reinforcement, is also implicated the development of disorders such as addiction, depression, and schizophrenia.[10,42−44] Dysregulation in dop-

https://doi.org/10.1021/acsomega.4c01322
ACS Omega 2024, 9, 33563−33573

aminergic signaling within this region can lead to maladaptive reward-seeking behaviors and motivational deficits. These neuropsychiatric disorders all have a prominent component of dopamine signaling dysfunction at their core; thus, it is necessary to possess tools, such as the models discussed herein, for studying, modeling, and predicting DA signaling behavior to better understand the physiology and pathophysiology of these disorders.

Developing such differential models to describe the kinetics of DA release from the synapse confers significant applications, both for advancing scientific understanding of DA neurotransmission, as well as for advancing clinical ability to treat neuropsychiatric disease. Changes or dysfunction in the dynamics of DA release are thought to play a pivotal role in regulating various physiological and behavioral processes, as well as leading to psychiatric diseases.[8,10,43,45,46] Models such as the ones discussed in this work can be utilized to explore how changes in synaptic parameters, neural activity, or external stimuli can impact DA release kinetics, and how changes in these kinetics are correlated with phenotypic or behavioral changes in the organism. Additionally, the ability to simulate and predict DA release patterns could enhance the development of targeted therapeutic interventions for neurological and psychiatric disorders associated with DA dysregulation, such as Parkinson's disease, schizophrenia, and addiction. Furthermore, the model's predictive capabilities may guide the optimization of drug treatments and aid in the design of novel therapeutic strategies, ushering in a new era of precision medicine in neurology and psychiatry.

5. CONCLUSIONS

In this work, we have outlined existing differential models for modeling DA release kinetics during FSCV experiments. By comparing the derivation and utility of each model on FSCV data acquired from our lab in two different brain regions from which FSCV data is often collected. Understanding the benefits and drawbacks of each model, as well as how to combine useful elements of separate models where appropriate, will guide optimal modeling and possible prediction of unseen DA release kinetics.

■ ASSOCIATED CONTENT

Supporting Information

The Supporting Information is available free of charge at https://pubs.acs.org/doi/10.1021/acsomega.4c01322.

> Four additional data sets that were analyzed using each model presented within the main text—two representing DA release into the dorsal striatum, one elicited by 60 Hz MFB stimulation and the other elicited by 90 Hz MFB stimulation, and two representing DA release into the nucleus accumbens, one elicited by 60 Hz VTA stimulation and the other elicited by 90 Hz VTA stimulation—with each data set taken from a different rat (six rats total across main text and supplement (PDF)

■ AUTHOR INFORMATION

Corresponding Authors

Hojin Shin − *Department of Neurologic Surgery and Department of Biomedical Engineering, Mayo Clinic, Rochester, Minnesota 55905, United States;* orcid.org/0000-0001-6095-5122; Email: shin.hojin@mayo.edu,

Yoonbae Oh − *Department of Neurologic Surgery and Department of Biomedical Engineering, Mayo Clinic, Rochester, Minnesota 55905, United States;* orcid.org/0000-0003-1779-978X; Email: oh.yoonbae@mayo.edu

Authors

Abhinav Goyal − *Mayo Clinic Medical Scientist Training Program, Mayo Clinic, Rochester, Minnesota 55905, United States; Department of Neurologic Surgery, Mayo Clinic, Rochester, Minnesota 55905, United States;* orcid.org/0000-0002-8465-7418

Una Karanovic − *Department of Neurologic Surgery and Mayo Clinic Graduate School of Biomedical Sciences, Mayo Clinic, Rochester, Minnesota 55905, United States*

Charles D. Blaha − *Department of Neurologic Surgery, Mayo Clinic, Rochester, Minnesota 55905, United States*

Kendall H. Lee − *Department of Neurologic Surgery and Department of Biomedical Engineering, Mayo Clinic, Rochester, Minnesota 55905, United States*

Complete contact information is available at: https://pubs.acs.org/10.1021/acsomega.4c01322

Author Contributions

A.G., K.H.L., and Y.O. conceived the study design. A.G. wrote the manuscript and code. A.G. and U.K. performed the data analysis. U.K., C.D.B., H.S., K.H.L., and Y.O. provided valuable guidance and manuscript edits. H.S. and Y.O. supervised all portions of the study and manuscript. All authors reviewed the results and approved the final version of the manuscript.

Notes

The authors declare no competing financial interest.

■ ACKNOWLEDGMENTS

This research was supported by the National Institutes of Health, NIH R01 NS112176, NS129549, and R42NS125895. Training grant funding for A.G. was supported by the NIH F30MH131254 and NIH T32GM065841-17.

■ REFERENCES

(1) Arbuthnott, G. W.; Wickens, J. Space, time and dopamine. *Trends in Neurosciences* **2007**, *30*, 62−69.

(2) Ungerstedt, U.; Pycock, C. Functional correlates of dopamine neurotransmission. *Bull. Schweiz Akad Med. Wiss* **1974**, *30*, 44−55.

(3) Beeler, J. A.; Daw, N. D.; Frazier, C. R. M.; Zhuang, X. Tonic Dopamine Modulates Exploitation of Reward Learning. *Front. Behav. Neurosci.* **2010**, *4*, 00170.

(4) Bergman, H.; Wichmann, T.; Karmon, B.; DeLong, M. R. The primate subthalamic nucleus. II. Neuronal activity in the MPTP model of parkinsonism. *Journal of Neurophysiology* **1994**, *72*, 507−520.

(5) Jokinen, P.; et al. Impaired cognitive performance in Parkinson's disease is related to caudate dopaminergic hypofunction and hippocampal atrophy. *Parkinsonism & Related Disorders* **2009**, *15*, 88−93.

(6) Calabresi, P.; Castrioto, A.; Di Filippo, M.; Picconi, B. New experimental and clinical links between the hippocampus and the dopaminergic system in Parkinson's disease. *Lancet Neurology* **2013**, *12*, 811−821.

(7) Martorana, A.; Koch, G. Is dopamine involved in Alzheimer's disease? *Frontiers in Aging Neuroscience* **2014**, *6*, 00252.

(8) Nobili, A.; Latagliata, E. C.; Viscomi, M. T.; Cavallucci, V.; Cutuli, D.; Giacovazzo, G.; Krashia, P.; Rizzo, F. R.; Marino, R.; Federici, M.; et al. Dopamine neuronal loss contributes to memory and reward dysfunction in a model of Alzheimer's disease. *Nat. Commun.* **2017**, *8*, 14727.

(9) Rusheen, A. E; Rojas-Cabrera, J.; Goyal, A.; Shin, H.; Yuen, J.; Jang, D.-P.; Bennet, K. E; Blaha, C. D; Lee, K. H; Oh, Y. Deep brain stimulation alleviates tics in Tourette syndrome via striatal dopamine transmission. *Brain* **2023**, *146*, 4174.
(10) Grace, A. A. Dysregulation of the dopamine system in the pathophysiology of schizophrenia and depression. *Nat. Rev. Neurosci* **2016**, *17*, 524−532.
(11) Cragg, S. J.; Rice, M. E. DAncing past the DAT at a DA synapse. *Trends in Neurosciences* **2004**, *27*, 270−277.
(12) Fuxe, K.; Agnati, L. F.; Marcoli, M.; Borroto-Escuela, D. O. Volume Transmission in Central Dopamine and Noradrenaline Neurons and Its Astroglial Targets. *Neurochem. Res.* **2015**, *40*, 2600−2614.
(13) Atcherley, C. W.; Wood, K. M.; Parent, K. L.; Hashemi, P.; Heien, M. L. The coaction of tonic and phasic dopamine dynamics. *Chem. Commun.* **2015**, *51*, 2235−2238.
(14) Guthrie, M.; Myers, C. E.; Gluck, M. A. A neurocomputational model of tonic and phasic dopamine in action selection: A comparison with cognitive deficits in Parkinson's disease. *Behavioural Brain Research* **2009**, *200*, 48−59.
(15) Venton, B. J.; et al. Real-time decoding of dopamine concentration changes in the caudate−putamen during tonic and phasic firing. *Journal of Neurochemistry* **2003**, *87*, 1284−1295.
(16) Schultz, W. Recent advances in understanding the role of phasic dopamine activity. *F1000Research* **2019**, *8*, 1680.
(17) Baur, J. E.; Kristensen, E. W.; May, L. J.; Wiedemann, D. J.; Wightman, R. M. Fast-Scan Voltammetry of Biogenic Amines. *Anal. Chem.* **1988**, *60*, 1268−1272.
(18) Budygin, E. A.; Kilpatrick, M. R.; Gainetdinov, R. R.; Wightman, R. M. Correlation between behavior and extracellular dopamine levels in rat striatum: comparison of microdialysis and fast-scan cyclic voltammetry. *Neurosci. Lett.* **2000**, *281*, 9−12.
(19) Heien, M. L. A. V.; Johnson, M. A.; Wightman, R. M. Resolving Neurotransmitters Detected by Fast-Scan Cyclic Voltammetry. *Anal. Chem.* **2004**, *76*, 5697−5704.
(20) Chang, S.-Y.; et al. Wireless Fast-Scan Cyclic Voltammetry to Monitor Adenosine in Patients With Essential Tremor During Deep Brain Stimulation. *Mayo Clinic Proceedings* **2012**, *87*, 760−765.
(21) Puthongkham, P.; Venton, B. J. Recent advances in fast-scan cyclic voltammetry. *Analyst* **2020**, *145*, 1087−1102.
(22) Moquin, K. F.; Michael, A. C. Tonic autoinhibition contributes to the heterogeneity of evoked dopamine release in the rat striatum. *Journal of Neurochemistry* **2009**, *110*, 1491−1501.
(23) Moquin, K. F.; Michael, A. C. An inverse correlation between the apparent rate of dopamine clearance and tonic autoinhibition in subdomains of the rat striatum: a possible role of transporter-mediated dopamine efflux. *J. Neurochem* **2011**, *117*, 133−142.
(24) Mitch Taylor, I.; Jaquins-Gerstl, A.; Sesack, S. R.; Michael, A. C. Domain-dependent effects of DAT inhibition in the rat dorsal striatum. *Journal of Neurochemistry* **2012**, *122*, 283−294.
(25) Taylor, I. M.; Ilitchev, A. I.; Michael, A. C. Restricted diffusion of dopamine in the rat dorsal striatum. *ACS Chem. Neurosci.* **2013**, *4*, 870−878.
(26) Shu, Z.; Taylor, I. M.; Michael, A. C. The dopamine patchwork of the rat nucleus accumbens core. *European Journal of Neuroscience* **2013**, *38*, 3221−3229.
(27) Vreeland, R. F.; et al. Biocompatible PEDOT:Nafion Composite Electrode Coatings for Selective Detection of Neurotransmitters in Vivo. *Anal. Chem.* **2015**, *87*, 2600−2607.
(28) Paxinos, G.; Watson, C. *The Rat Brain in Stereotaxic Coordinates*; Elsevier, 2006.
(29) Lee, K. H.; Lujan, J. L.; Trevathan, J. K.; Ross, E. K.; Bartoletta, J. J.; Park, H. O.; Paek, S. B.; Nicolai, E. N.; Lee, J. H.; Min, H.-K.; et al. WINCS Harmoni: Closed-loop dynamic neurochemical control of therapeutic interventions. *Sci. Rep.* **2017**, *7*, 46675.
(30) Walters, S. H.; Taylor, I. M.; Shu, Z.; Michael, A. C. A Novel Restricted Diffusion Model of Evoked Dopamine. *ACS Chem. Neurosci.* **2014**, *5*, 776−783.
(31) Walters, S. H.; Robbins, E. M.; Michael, A. C. Modeling the Kinetic Diversity of Dopamine in the Dorsal Striatum. *ACS Chem. Neurosci.* **2015**, *6*, 1468−1475.
(32) Wightman, R. M.; May, L. J.; Michael, A. C. Detection of Dopamine Dynamics in the Brain. *Anal. Chem.* **1988**, *60*, 769A.
(33) Hrabětová, S.; Nicholson, C. Contribution of dead-space microdomains to tortuosity of brain extracellular space. *Neurochem. Int.* **2004**, *45*, 467−477.
(34) Nicholson, C. Interaction between diffusion and Michaelis-Menten uptake of dopamine after iontophoresis in striatum. *Biophys. J.* **1995**, *68*, 1699−1715.
(35) Hrabetova, S.; Masri, D.; Tao, L.; Xiao, F.; Nicholson, C. Calcium diffusion enhanced after cleavage of negatively charged components of brain extracellular matrix by chondroitinase ABC. *J Physiol.* **2009**, *587*, 4029−4049.
(36) Bath, B. D.; et al. Subsecond Adsorption and Desorption of Dopamine at Carbon-Fiber Microelectrodes. *Anal. Chem.* **2000**, *72*, 5994−6002.
(37) Trevathan, J. K.; et al. Computational Modeling of Neurotransmitter Release Evoked by Electrical Stimulation: Nonlinear Approaches to Predicting Stimulation-Evoked Dopamine Release. *ACS Chem. Neurosci.* **2017**, *8*, 394−410.
(38) Natori, S.; et al. Subsecond reward-related dopamine release in the mouse dorsal striatum. *Neuroscience Research* **2009**, *63*, 267−272.
(39) Carboni, E.; Imperato, A.; Perezzani, L.; Di Chiara, G. Amphetamine, cocaine, phencyclidine and nomifensine increase extracellular dopamine concentrations preferentially in the nucleus accumbens of freely moving rats. *Neuroscience* **1989**, *28*, 653−661.
(40) de Jong, J. W.; et al. Reducing Ventral Tegmental Dopamine D2 Receptor Expression Selectively Boosts Incentive Motivation. *Neuropsychopharmacol* **2015**, *40*, 2085−2095.
(41) Brittain, J.-S.; Brown, P. Oscillations and the basal ganglia: motor control and beyond. *Neuroimage* **2014**, *85*, 637−647.
(42) Heifets, B. D.; Salgado, J. S.; Taylor, M. D.; Hoerbelt, P.; Cardozo Pinto, D. F.; Steinberg, E. E.; Walsh, J. J.; Sze, J. Y.; Malenka, R. C. Distinct neural mechanisms for the prosocial and rewarding properties of MDMA. *Science Translational Medicine* **2019**, *11*, aaw6435.
(43) Yuen, J.; et al. Cocaine-Induced Changes in Tonic Dopamine Concentrations Measured Using Multiple-Cyclic Square Wave Voltammetry in vivo. *Front Pharmacol* **2021**, *12*, 705254.
(44) Yuen, J.; et al. Cocaine increases stimulation-evoked serotonin efflux in the nucleus accumbens. *Journal of Neurophysiology* **2022**, *127*, 714−724.
(45) Yuen, J.; et al. Deep Brain Stimulation for Addictive Disorders—Where Are We Now? *Neurotherapeutics* **2022**, *19*, 1193−1215.
(46) Lecourtier, L.; DeFrancesco, A.; Moghaddam, B. Differential tonic influence of lateral habenula on prefrontal cortex and nucleus accumbens dopamine release. *Eur. J. Neurosci* **2008**, *27*, 1755−1762.

https://doi.org/10.1021/acsomega.4c01322
ACS Omega 2024, 9, 33563−33573